Journal of the Korean Society for Nondestructive Testing
Vol. 29, No. 4 (2009. 8)

Development of Ultrasonic Wave Propagation Imaging System

Chen-Ciang Chia*, Jung-Ryul Lee*† and Jong Heon Kim**

Abstract Laser-based ultrasonic sensing requires the probe with fixed focal length, but this requirement is not essential in laser-based ultrasonic generation. Based on this fact, we designed a pulsed laser-based ultrasonic wave propagation imaging (UWPI) system with a tilting mirror system for rapid scanning of target, and an in-line band-pass filtering capable of ultrasonic mode selection. 1D-temporal averaging, 2D-spatial averaging, and 3D-data structure building algorithms were developed for clearer results allowing for higher damage detectability. The imaging results on a flat stainless steel plate were presented in movie and snapshot formats which showed the propagation of ultrasound visible as a concentric wavefield emerging from the location of an ultrasonic sensor. A hole in the plate with a diameter of 1 mm was indicated by the scattering wavefields. The results showed that this robust UWPI system is independent of focal length and reference data requirements.

Keywords: Q-Switched Pulsed Laser, Laser Ultrasonics, Ultrasonic Wave Propagation Imaging, Nondestructive Test and Evaluation

1. Introduction

Structural health monitoring (SHM) systems and their counterparts, nondestructive inspection (NDI) systems, have been an essential part of the new structural components for safer operation and lower maintenance costs. Various SHM and NDI technologies have been developed for different materials and applications, and every method has its own advantages and disadvantages. Among them, ultrasound has been widely used for both SHM and NDI applications because ultrasonic waves are sensitive to most flaws, are not radiation hazardous, and provide many features for flaw characterization. This method itself has branched into several approaches, including the phased-array and time-of-flight diffraction approaches, and some ultrasonic imaging approaches have also been adopted for easier interpretation of results. The phase array ultrasound has attracted much attention because of its flexibility in varying the angle of inspection and in focusing the beam to a point of interest (Satyanarayan et al., 2007; Song et al., 2002). The time-of-flight diffraction approaches, on the other hand, have become a promising NDI for damage detection in certain applications, for example in pressure vessels (Raj et al., 2006). Ultrasonic imaging has also achieved some significant advancements, for example in image quality improvement through the use of the synthetic aperture focusing technique (Sicard et al., 2002; Spies and Jager, 2003). The application of these approaches is limited due to their requirement of a contact transducer. Laser-based ultrasonic NDI has been introduced to overcome this shortcoming. Laser-based ultrasonic generation and detection

Received: May 7, 2009, Revised: August 3, 2009, Accepted: August 10, 2009. *Department of Aerospace Engineering, Chonbuk National University, 664-14, Duckjin-dong, Jeonju, Chonbuk 561-756, Korea, **Aeronautical Technology Directorate, Agency for Defense Development, Yuseong-gu, P.O. Box 35-7, Daejeon, 305-600, Korea, †Corresponding Author: leejrr@chonbuk.ac.kr

offers many advantages (Fomitchov et al., 2004; Scruby and Drain, 1990; Huber et al., 2000) including (i) non-contact in-situ measurements, (ii) remote placement of equipment for use in hostile environments, including the inspection of targets containing dangerous materials or under elevated temperature, (iii) high spatial resolution, and (iv) the ability to inspect surfaces with complex geometry. The acoustic wavefield imaging technique (Michaels and Michaels, 2006), called ultrasonic wave propagation imaging (UWPI) in this paper, is based on the scanning of an air-coupled transducer, but requires a fixed focal length and a small measurement distance (millimeter range). The focal length requirement greatly reduces the robustness of the system for scanning surfaces with complex curves, as a specially tailored scanning system will be required to fix the focal length of the laser or the non-contact transducer. Another UWPI technology was realized using a scanning laser Doppler vibrometer and a fixed piezoelectric ultrasonic transmitter (Staszewski et al., 2007). Noncontact remote scanning was possible, but images with a low spatial resolution were acquired because only 405 points were scanned in a region of 110×60 mm^2 due to the focusing requirement and slow scanning speed. In addition, the use of the laser Doppler vibrometer with scanning and focusing modules dramatically increased the system cost compared to the system based on an air-couple transducer. In the same year, a reciprocal set-up was introduced in which a scanning Q-switched pulsed laser and a fixed piezoelectric receiver were used instead of the piezoelectric transmitter and scanning laser vibrometer (Yashiro et al., 2008). This was applied to a drill, an elbow pipe joint, an impact damaged CFRP plate, and metal and composite skin-stringer structures (Lee et al., 2007a; Lee et al., 2007b). The SHM methodology stimulating the integrated sensor network using the UWPI system was also demonstrated.

In this paper, we introduce a new design and algorithm for the UWPI system. The present UWPI system utilizes a Q-switched pulsed laser (QPL) to generate the ultrasound on the target as in the previous contributions (Yashiro et al., 2008; Lee et al., 2007a; Lee et al., 2007b). Then an ultrasonic receiver installed either on the scanning surface or on the back of the target captures the waveforms when the laser scans through the area of interest. Stored waveforms are processed and displayed as a movie or consecutive time slices. Propagating waves are visible as a concentric wavefield emerging from the sensing point. Any discontinuity in the target along the propagation path between the impinging point and the sensing point will alter the ultrasound wave through mode conversion, reflection, diffraction, and scattering. This UWPI system utilizes a tilting mirror system (TMS) for rapid maneuvering of the laser impinging point instead of scanning a bulky laser head as in the previous system (Yashiro et al., 2008; Lee et al., 2007a), and is capable of scanning and presenting a scanning result within 40 minutes (37 min for scanning, and 3 min for result display) for a square region of 100 mm×100 mm (40401 points). This scanning speed is 3.5 times faster, and the post-imaging processing is 10 times faster than in the previous system. In-line real time filtering in frequency domain is now included, and is used to reduce the number of wave cycles and select appropriate ultrasonic modes. This is an effective way to improve the visibility of the effect of a defect on wave propagation by gating the ultrasonic modes with respect to the broadband input generated by the pulsed laser. Also, parallel-signal averaging in the time domain, and post-image smoothing in the spatial domain increase the damage detectability of the system by increasing the signal-to-noise (SNR) ratios of 1D waves and the 2D wavefield. These points are presented in the section on the system design and signal processing algorithm. We then demonstrate the

application of the method to the detection of artificial damage on flat surfaces. Unlike the previous demonstrations of UWPI (Michaels and Michaels, 2006; Staszewski et al., 2007; Yashiro et al., 2008; Lee et al., 2007a; Lee et al., 2007b), we demonstrate the detection of a very small hole.

2. Methodology

Fig. 1 shows the schematic of the UWPI system. The system is comprised of a Nd:YAG QPL with a wavelength of 1064 nm, a near field beam diameter of 2.8 mm, and a divergence of 1.37 mrad, a motorized TMS with a maximum angle of 0.1171 rad and with a maximum angular speed of 0.0107 rad/s, a PZT sensor with a central frequency of 350 kHz along with its amplifier and power supply unit, a programmable filter, a digital oscilloscope, and a computer with LabVIEW^{TM} for hardware control, waveform acquisition, and image processing. The TMS consists of a laser mirror with a working wavelength band of 1047-1064 nm, and two motorized translation cylinders for tilting about the x and y axes as shown in Fig. 2. We consider an area of interest for inspection that measures L_V and L_H unit lengths in the vertical and horizontal directions, respectively (Fig. 3(a)). The QPL system fires optical pulses with a duration of 8 ns at a repetition of 20 Hz, and approximately 15 mJ of energy at the mirror. The TMS tilts such that the laser beam scans vertically downward, steps horizontally at the

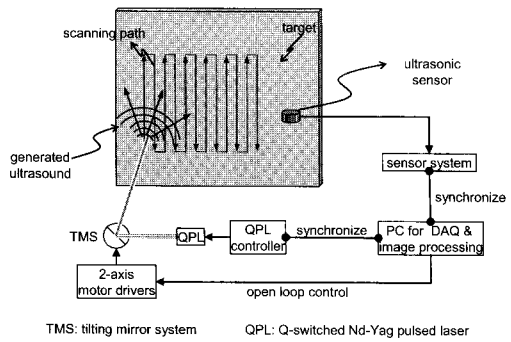

Fig. 1 Schematic diagram of the ultrasonic wave propagation imaging (UWPI) system

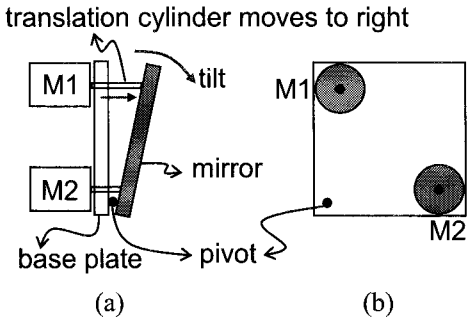

Fig. 2 Schematic and working principle of TMS. (a) side view, (b) front view. The motor M1 and M2 are responsible for vertical and horizontal tilting, respectively

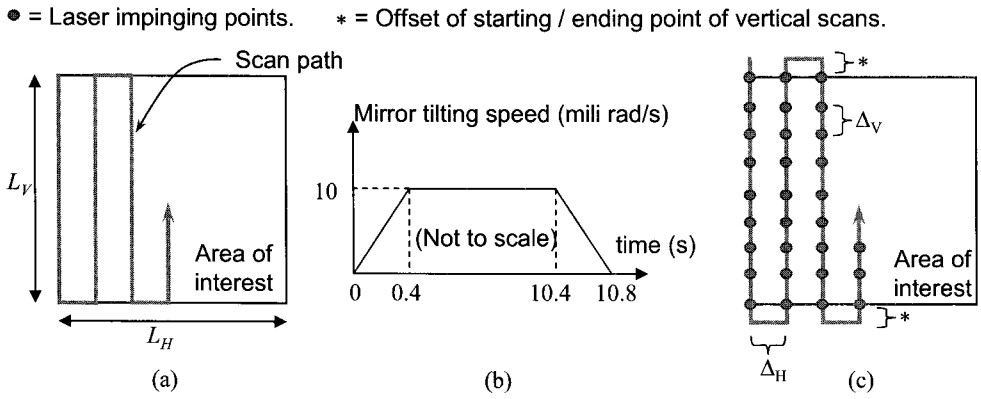

Fig. 3 Area of interest for scanning, (a) original scanning path, (b) speed profile of TMS when distance of TMS from target is 1 m, and (c) modified scanning path for mirror acceleration and deceleration. Laser fires only within or on the edge of the area of interest

end of the downward movement, and then tilts upward for the next vertical scan, as shown in Fig. 3(a). The process continues until the area of interest is fully scanned. To fix the vertical scanning interval, $\triangle_V$, the tilting speed of the mirror during the vertical movement must be constant because the laser firing frequency is constant at a given setting. However, the TMS has the speed profile shown in Fig. 3(b). Considering the acceleration requirement from zero velocity at the starting point, to a constant velocity followed by deceleration at the ending point of every vertical movement, an acceleration and deceleration buffer zone must be included in the system. Hence, the starting and ending points of every vertical movement are offset outside the area of interest, as shown in Fig. 3(c). The QPL is controlled to be fired only when the scanning path is within the area of interest or on its edges.

When the laser beam impinges on the surface of the target, the affected part of the target expands thermoelastically and creates an ultrasonic wave. The wave propagates through the target and reaches the PZT sensor bonded on its surface. The sensor can be installed on the same side or on the opposite side of the scanning. A non-contact ultrasonic sensor can be utilized, depending on the accessibility of the target structure. The signal from the sensor is amplified, filtered, shown on an oscilloscope, and then stored in the computer through LabVIEW™ data acquisition. One waveform is stored for each laser impinging point. An illustration of the waveform is shown in Fig. 4(a) and is saved in a spreadsheet with the row direction being the time axis. The waveform for each subsequent impinging point along one vertical scan is stored as a new column on the same spreadsheet, as

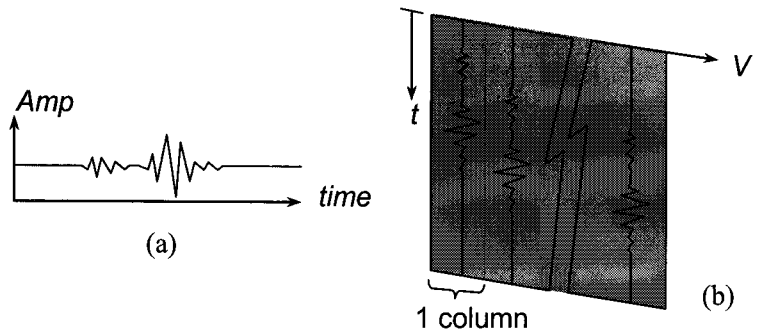

Fig. 4 Illustration of (a) signal saved, and (b) data structure on spreadsheet

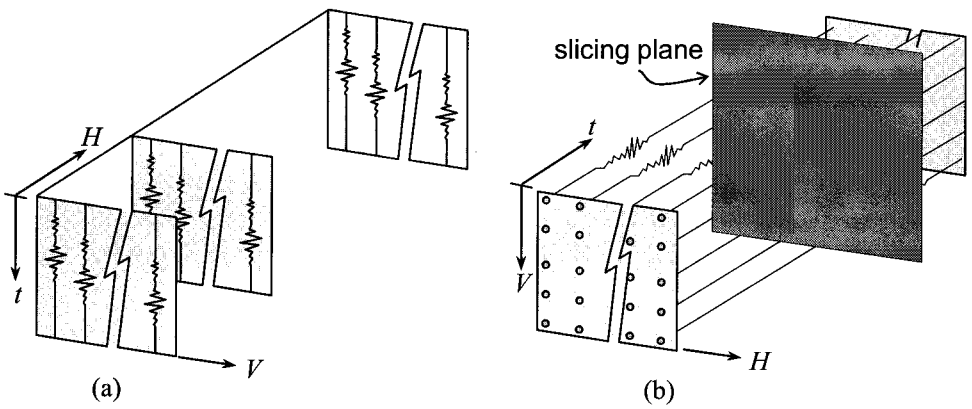

Fig. 5 Illustration of data processing algorithm, (a) The raw data structure on spreadsheet where each spreadsheet stores the data for one vertical scan, (b) Data being manipulated to this structure and sliced along the time axis

shown in Fig. 4(b). Hence there is one spreadsheet for each vertical scan containing the waveforms for all of the impinging points along the scan. Collecting the data from all vertical scans for the whole area of interest creates the 3D data structure shown in Fig. 5(a).

The objective of post processing is to show the results in movie and image forms. The first step of the post processing is the arrangement of the data so that one spreadsheet corresponds to one image snapshot in the movie result, while one data point on each spreadsheet corresponds to one pixel of the image frame. The required UWPI data structure can be obtained by rotating the data from the arrangement shown in Fig. 5(a) to the arrangement shown in Fig. 5(b). The data is then sliced along the time-axis so that each slice of data physically maps the ultrasonic magnitude at every laser impinging point on the area of interest. Then, the consecutive spreadsheets are the ultrasonic magnitude map of the area of interest at different propagation times. These can be conveniently plotted on intensity maps using a color scheme. Successively loading the spreadsheet data into an intensity map creates an ultrasonic wave propagation movie (UWPM) of the area of interest. Every intensity map becomes one image snapshot from the movie.

The raw UWPM is often adequate, but when the damage-induced wave is difficult to be isolated, for example when the SNR is low, filtering or adjacent averaging can be useful. The ideal ultrasound wave in this UWPM is a wave with only one peak. This is because an excessive number of wavefronts in the final image or movie will potentially mask the damage-induced wave causing the inspector to overlook it, as will be shown in the discussion of the results. An adjustable band-pass filter can be used to minimize this problem. Two data averaging functions, temporal averaging and spatial averaging, were also included in the data processing algorithm as optional functions. When selected, temporal averaging works to smooth the raw 1D ultrasound signal in the time domain using any greater-than-one odd number of adjacent points for averaging, based on the selection of the user. For this process, additional time is not required because the waveform scanned just before the present scanning point is processed in parallel, independent of the scanning control. On the other hand, spatial averaging option can be selected as a post-image processing just before loading the spreadsheet data into the intensity map plot. The spatial averaging performs averaging on the data of n×n adjacent points an arbitrary number of times (k) instead of using a large kernel one time, where n is chosen for a small kernel, for examples, 3, 5. This iterative spatial averaging result in a Gaussian kernel instead of a box kernel in the case of the large kernel one time (Lee, 2005). Uses of these filtering and averaging functions are based on the system user's discretion. The flow chart of the total UWPI algorithm is given in Fig. 6.

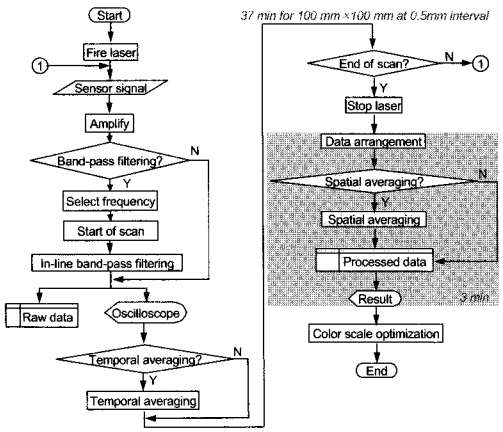

Fig. 6 Flow chart of the UWPI data acquisition and processing algorithm

The maximum scanning path length $L_{\max}$, the maximum scanning points spatial interval $\triangle_{\max}$, and the minimum scanning points spatial interval $\triangle_{\min}$ are theoretically given as follows:

$$L_{max} = 0.2268D \quad (1)$$

$$\triangle_{max} = 1.070 \times 10^{-3} D \quad (2)$$

$$\triangle_{min} = 1.1 \times 10^{-5} D \quad (3)$$

where D is the distance of the TMS from the target, and D≥500 mm in the system designed in this paper. Placing the TMS at the nearest distance to the target (500 mm) will give a maximum effective scanning area of 113×113 mm^2 with a minimum scanning interval of 0.0055 mm. The scanning point spatial interval $\triangle$ will be the initial spatial resolution of the ultrasonic propagation snapshot. Placing the TMS 20 m from the target gives a minimum scanning interval of 0.22 mm, which is still considered to provide a good scanning resolution.

3. Experiment Setup

To illustrate the methodology described in the preceding section, consider a stainless steel plate measuring 500×500×1 mm with an open hole of diameter ϕ=1 mm drilled at the centre to simulate damage. The TMS was programmed such that the centre of a scanning area of 100×100 mm^2 coincided with the hole location. Using the same vertical and horizontal scan interval $\triangle_V=\triangle_H$=0.5 mm, 40401 waveforms corresponding to all the laser impinging points were stored. The mirror was placed at a distance of 1 m, directly opposite the area of interest. In this set up, the PZT sensor was bonded to the opposite side of the scanning surface. As viewed from the side of the scan, it was located in the lower right quadrant, away from the horizontal symmetrical line of the scan area. The oscilloscope was set at a sampling rate of 2.5 MSa/s, and fast triggering 500 points. Using this oscilloscope setting, the first 150 data points of the waveforms were sufficient to produce a full UWPM. Hence, the LabVIEW™ data acquisition program was set to save only 150 points for every waveform. In this paper, a programmable filter was incorporated to search for a filtering frequency that provided the minimum number of peaks in the waveform. It was found that a band-pass of 330-340 kHz was the best for the specimen and sensor used. Three inspection cases are presented in this paper. In case 1, the effect of the band-pass filtering was investigated. In case 2, the 330-340 kHz band-pass filter was used, and the effect of three points temporal averaging was investigated. In case 3, we looked into the effect of spatial averaging. The signals were filtered by the 330-340 kHz band-pass filter, and then smoothed by repeating 3×3 spatial averaging two times before plotting the intensity map.

4. Results

The results for each inspection were ready 40 minutes after beginning the scan, which consisted of 37 minutes for scanning and 3 minutes for 3D data-building and post-image processing for UWPM. The results of case 1 were given in snapshots from the UWPM in Fig. 7. Fig. 7(a) shows the sensor and the hole at the back of the plate. This photo was mirrored left to right for ease of comparison with the snapshots. Fig. 7(b) and (c) show the snapshots at 12.00 μs and 26.00 μs for the raw data with neither filtering nor averaging. The propagating ultrasound is visible as a concentric wavefield emerging from the bonded PZT sensor in Fig. 7(b). Scattered wave due to the interaction of the propagating wave with the small hole can hardly be detected in Fig. 7(c) because the damage-induced waves were partially masked. The use of the band-pass filter reveals more of the damage-induced wave, as shown in Figs. 7(f) and (g).

Fig. 8 shows the results for inspection case 2. The snapshot at 30.00 μs with band-pass filtering but without temporal averaging was given in Fig. 8(a). When three points temporal averaging were used, the visibility of the damage-induced wave was slightly increased, as shown in Fig. 8(b). Their time domain signal corresponds to coordinate (25, 25) mm was given in Fig. 8(c) and (d), respectively.

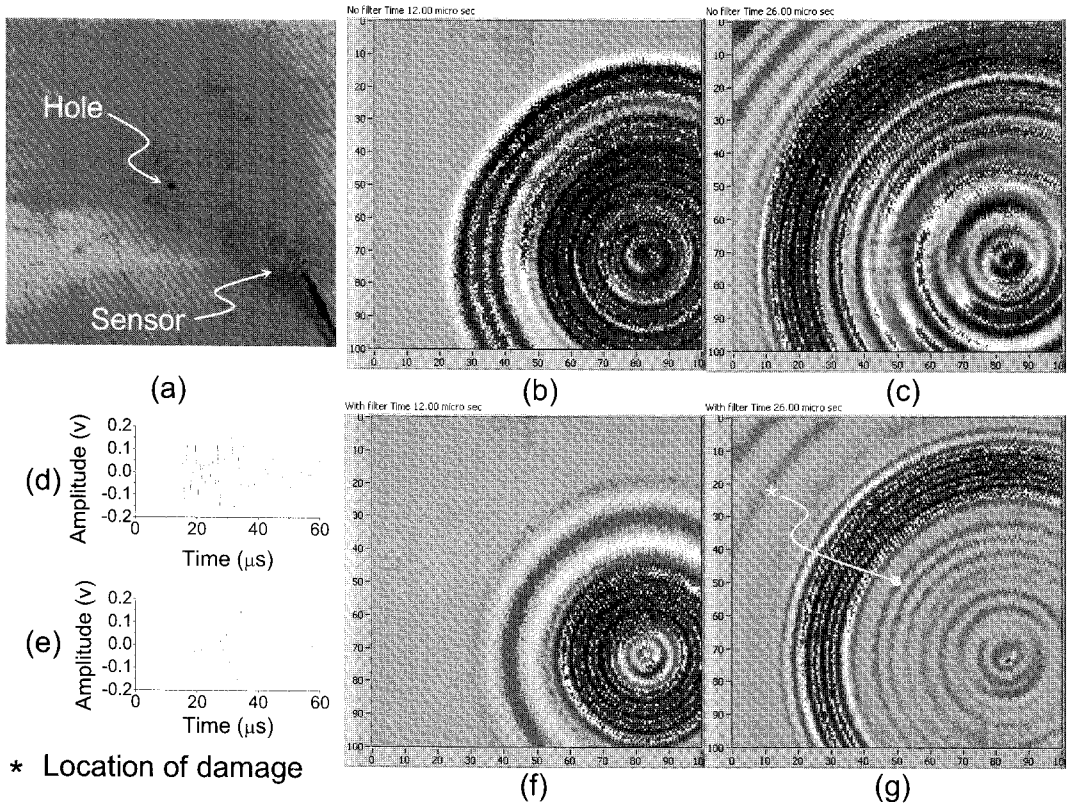

Fig. 7 Snapshots from the UWPM. (a) The target with hole and sensor bonded. (b) Wavefield seen as if emerging from the sensor. (c) Damage-induced wave can hardly be identified. Time domain signal at coordinate (25, 25) mm for cases of (d) without, and (e) with band-pass filtering. (f) and (g) are the counterpart snapshots for (b) and (c) after band-pass filtering. Damage-induced wave can be identified as if emerging from the location of damage

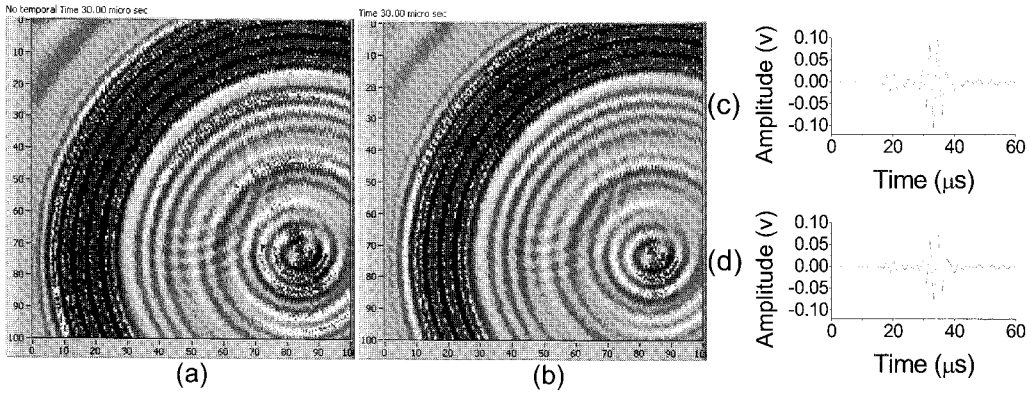

Fig. 8 Results for inspection case 2. Snapshot at 30.00 μs for situation (a) without temporal averaging, and (b) with 3 points temporal averaging. Their time domain signal corresponds to coordinate (25, 25) mm is given in (c) and (d), respectively

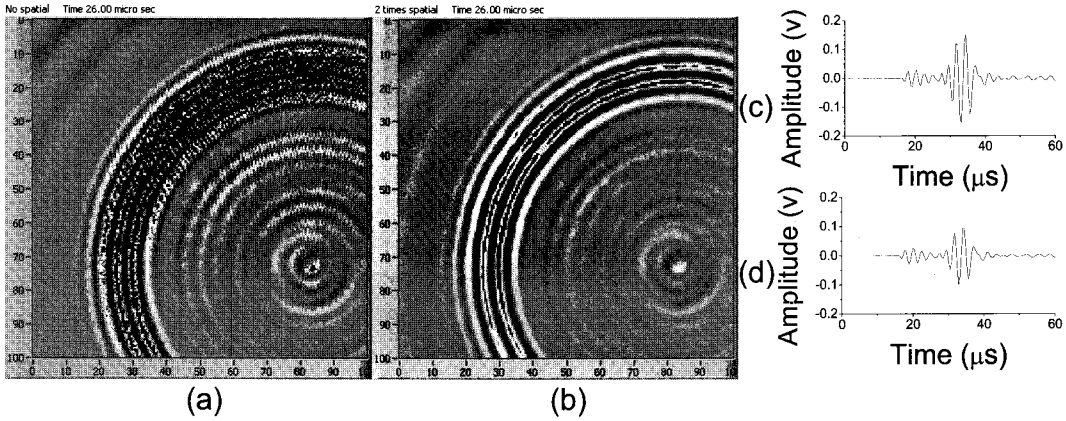

Fig. 9 Result of inspection case 3. Snapshots at 26.00 μs for situation (a) without spatial averaging, and (b) with 2 times spatial averaging, together with the time domain signal at coordinate (25, 25) mm for situation (c) without spatial averaging, and (d) with 2 times spatial averaging. (UWPM is available for Fig. 9)

Fig. 9 shows the results of case 3, where a snapshot without the use of spatial averaging, and a snapshot with the use of two repeats of the 3×3 spatial averaging (3×3_2) are shown in Figs. 9(a) and (b), respectively. Although the damage was detected successfully in Fig. 9(a), it could be missed due to the coarse image quality. Fig. 9(b), on the other hand, is much smoother and shows that the spatial averaging is useful in producing clearer snapshots or UWPM, which is available together with Fig. 9. The execution of the temporal averaging and spatial averaging functions in the UWPI algorithm requires less than 10 seconds. Its addition to the total inspection time is negligible considering the advantages shown.

The investigation of the UWPI system and algorithm above concludes that the system can be used to detect and locate damage and material defects. The results in movie form can be used to see more details of the target structure condition through inspection of the propagation of the ultrasonic waves.

5. Discussion

The UWPI system provides good results, but the best final result is not always guaranteed as there are several performance-related issues to address including the resolution, smoothness, and SNR ratio. The spatial resolution for each image snapshot is governed by the number of laser impinging points on the area of interest. A very small scanning interval was not considered in this paper dealing with SHM or NDT, but the laser beam diameter with a Gaussian intensity distribution will be an important factor in the determination of spatial resolution. It can be seen intuitively that one can increase the number of laser impinging points within the area of interest by decreasing the value of the scanning intervals $\triangle_V$ and $\triangle_H$. In contrast, for example, it took 37 min to scan an area of 100×100 mm^2 with a 0.5 mm interval. If one scanned 200×200 mm^2 with a 1mm interval, the scan would also take 37 min, but the initial spatial resolution would be deteriorated by a factor of two.

6. Conclusions

A robust UWPI system was designed. The system is capable of faster scanning due to TMS and ultrasonic mode selection which become possible due to a real-time band-pass filter. Versatile functions for the UWPI algorithm were developed: a temporal averaging to be performed in parallel with the scan, and a spatial averaging performed as post-image processing. The new

design and algorithm enabled the scanning speed to increase to 9.0 mm·point/s, and allowed the post-image processing time to decrease to 3 min for 40401 points. The UWPI system is a simple and yet robust damage inspector. A minimum amount of training is required to identify the damage-induced waves from the wave propagation movie or from snapshots produced by the UWPI system. The system was applied to a flat stainless steel plate and a small hole with a diameter of 1mm was successfully localized. Thirty seven minutes of scanning time and three minutes of result processing time were needed. The results showed that the temporal averaging and spatial averaging functions included in the UWPI system were useful. The use of TMS and the capability of expanding the system for parallel scanning using a beam splitter can greatly reduce the scanning time with little increase in financial cost.

Acknowledgements

We performed this study under the applied research project (UC080019JD) which is supported by ADD (Agency for Defense Development) in Korea

References

Fomitchov, P. A., Kromin, A. K., Krishnaswamy, S. and Achenbach, J. D. (2004) Imaging of Damage in Sandwich Composite Structures Using a Scanning Laser Source Technique, *Composites: Part B*, Vol. 35, pp. 557-562

Huber, R. D., Candy, J. V. and Chambers, D. H. (2000) *Review of Progress in Quantitative Nondestructive Evaluation*, in: D. O. Thompson and D. E. Chimenti (Eds.), AIP Conference Proceeding, Vol. 509, American Institute of Physics, New York, pp. 859-864

Lee, J. R. (2005) Spatial Resolution And Resolution in Phase-Shifting Laser Interferometry, *Measurement Science and Technology*, Vol. 16, pp. 2525-2533

Lee, J. R., Takatsubo, J. and Toyama, N. (2007). Disbond Monitoring at Wing Stringer Tip Based on Built-in Ultrasonic Transducers and a Pulsed Laser, *Smart Materials and Structures*, Vol. 16, pp. 1025-1035

Lee, J. R., Takatsubo, J., Toyama, N. and Kang, D. H. (2007) Health Monitoring of Complex Curved Structures Using an Ultrasonic Wavefield Propagation Imaging System, *Meas. Sci. Technol.*, Vol. 18, pp. 3816-3824

Michaels, T. E. and Michaels, J. E. (2006) Application of Acoustic Wavefield Imaging to Non-Contact Ultrasonic Inspection of Bonded Components, *Review of Quantitative Nondestructive Evaluation*, Vol. 25, pp. 1484-1491

Raj, B., Mukhopadhyay, C. K. and Jayakumar, T. (2006) Frontiers in NDE Research Nearing Maturity for Exploitation to Ensure Structural Integrity of Pressure Retaining Components, *Pressure Vessels and Piping*, Vol. 83, pp. 322-335

Satyanarayan, L., Sridhar, C., Krishnamurthy, C. V. and Balasubramaniam, K. (2007) Simulation of Ultrasonic Phased Array Technique for Imaging and Sizing of Defects Using Longitudinal Waves, *Pressure Vessels and Piping*, Vol. 84, pp. 716-729

Scruby, C. B. and Drain, L. E. (1990) *Laser Ultrasonics*: Techniques and Applications, Adam Hilder, New York, Vol. 1, Chap. 1, pp. 6

Sicard, R., Goyette, J. and Zellouf, D. (2002) A SAFT Algorithm for Lamb Wave Imaging of Isotropic Plate-Like Structures, *Ultrasonics*, Vol. 39, pp. 487-494

Song, S. J., Shin, H. J. and Jang, Y. H. (2002) Development of an Ultrasonic Phased Array System for Nondestructive Tests of Nuclear Power Plant Components, *Nuclear Engineering and Design*, Vol. 214, pp. 151-161

Spies, M. and Jager, W. (2003) Synthetic Aperture Focusing for Defect Reconstruction in Anisotropic Media, *Ultrasonics*, Vol. 41, pp. 125-131

Staszewski, W. J., Lee, B. C. and Traynor, R. (2007) Fatigue Crack Detection in Metallic Structures with Lamb Waves and 3D Laser Vibrometry, *Measurement Science and Technology*, Vol. 18, pp. 727-739

Yashiro, S., Takatsubo, J., Miyauchi, H. and Toyama, N. (2008) A Novel Technique for Visualizing Ultrasonic Waves in General Solid Media by Pulsed Laser Scan, *NDT&E International*, Vol. 41, pp. 137-144